Geobiology

Redox heterogeneity of subsurface waters in the Mesoproterozoic ocean

Journal:	*Geobiology*
Manuscript ID:	Draft
Manuscript Type:	Standard Research Paper
Key Words:	Mesoproterozoic, redox, oxygen, Kaltasy Formation, microfossils, Russia

Redox heterogeneity of subsurface waters in the Mesoproterozoic ocean

Keywords: Mesoproterozoic; redox; oxygen; Kaltasy Formation; microfossils; Russia

Number of words in text: 5,659
Number of tables: 1
Number of Figures: 4
Number of Supplemental files: 3

[1] *The authors do not have any conflicts of interest.*

A substantial body of evidence suggests that subsurface water masses in mid-Proterozoic marine basins were commonly anoxic, either euxinic (sulfidic) or ferruginous (free ferrous iron). To further document redox variations during this interval, a multi-proxy geochemical and paleobiological investigation was conducted on the ~1000 meter thick Mesoproterozoic (Lower Riphean) Arlan Member of the Kaltasy Formation, central Russia. Iron speciation geochemistry, organic geochemistry, redox-sensitive trace element abundances, and pyrite sulfur isotope values all indicate that basinal calcareous shales of the Arlan Member were deposited beneath an oxygenated water column, and, consistent with this interpretation, eukaryotic microfossils are abundant in basinal facies. The Rhenium-Osmium (Re-Os) systematics of the Arlan shales yield depositional ages of 1414 ± 40 Ma and 1427 ± 43 Ma for two horizons near the base of the succession, consistent with previously proposed correlations. The presence of free oxygen in a deep basinal environment adds an important end-member to Proterozoic redox heterogeneity, requiring explanation in light of previous data from time-equivalent basins. Very low total organic carbon contents in the Arlan Member are perhaps the key – oxic deep waters are more likely (under any level of atmospheric O_2) in oligotrophic systems with low export production. Documentation of a full range of redox heterogeneity in subsurface waters and the existence of local redox controls indicate that no single stratigraphic section or basin can adequately capture both the mean redox profile of Proterozoic oceans and its variance at any given point in time.

INTRODUCTION

How the Earth's atmosphere and ocean transitioned from their early, essentially anoxic state to our familiar oxygen-rich world remains controversial. It is well documented that an oxygenation event at ~2400 Ma (Ma: million years) established a persistently oxic atmosphere and surface ocean, but deep ocean chemistry remains uncertain through the remainder of the Proterozoic Eon (Kah and Bartley, 2011). Geologists long posited that the widespread disappearance of banded iron formation at ~1800 Ma reflects oxygenation of the deep ocean (Holland, 1984); however, Canfield (1998) proposed that under relatively low atmospheric O_2, the deep ocean would remain anoxic and indeed become euxinic, reflecting increased rates of bacterial sulfate reduction at depth. The nature of subsurface ocean chemistry is critical to our understanding of Earth surface history and biological evolution.

Initial tests of the Canfield hypothesis were supportive: iron geochemical studies of the McArthur and Roper basins (data from ~1730-1630 Ma and ~1500-1400 Ma, respectively) in northern Australia indicated that basinal euxinia existed beneath an oxic mixed layer through an interval more than 300 million years long (Shen et al., 2002, 2003). Indeed, Poulton et al. (2004) argued that rocks of the Animikie Basin, Ontario, captured a global transition from ferruginous to sulfidic subsurface waters roughly 1800 million years ago. Subsequent organic geochemical research corroborated these findings, documenting biomarker molecules for green- and purple-sulfur bacteria in the 1640 Ma Barney Creek Formation of the McArthur Basin, a finding that requires euxinia within the photic zone (Brocks et al., 2005). Studies of molybdenum isotopes, which track the

percentage of seafloor bathed in euxinic waters, also pointed to more widespread sulfidic conditions than in the modern ocean (Arnold et al., 2004; Kendall et al., 2009).

Tracers based on the abundance and/or isotopic composition of Mo and other redox sensitive trace metals (e.g., Partin et al., 2013) are extremely useful in understanding how the mean state of the ocean has changed through time, but they do not address the question of variance among basins. Continuing studies of mid-Proterozoic sedimentary environments using local proxies (those that record conditions in the immediately overlying water-column) have pointed to a more nuanced picture of sub wave-base ocean chemistry, documenting both euxinic and ferruginous conditions within the same basin. Cores from both the Animikie (Poulton et al., 2010) and McArthur basins (Planavsky et al., 2011) demonstrate heterogeneity in deep ocean chemistry—S^{2-} and Fe^{2+} are mutually exclusive in space but not in time. Similar features are also observed in more extensively studied Neoproterozoic successions, where it now appears that euxinia is the exception rather than the rule (Canfield et al., 2008, Johnston et al., 2010; Sperling et al 2013). Johnston et al. (2010) proposed a model for the development of euxinia, noting that oscillations between ferruginous and euxinic conditions in basinal strata track sedimentary total organic carbon contents, which suggests that euxinia is most likely to develop when organic carbon delivery exceeds the delivery of electron acceptors that outcompete sulfate (e.g. nitrate, ferric iron; see also Planavsky et al., 2011; Sperling et al., 2013). Adding to this emerging heterogeneity, data from mineral assemblages suggest that despite widespread anoxia in oxygen minimum zones, dysoxia (oxygen present but at low levels) apparently persisted in the deepest parts of at least some mid-Proterozoic oceans (Slack et al., 2007; 2009).

Here we report multi-proxy sedimentary geochemical and paleobiological analyses of lower Mesoproterozoic strata recovered by the 203 Bedryazh drill core from the Volgo-Ural region, Russia (Fig. 1A), drilled about 5 km south-west from Bedryazh settlement (Google Map Coordinates, decimal degrees latitude and longitude, 56.3430 N lat., 55.5302 E long.). To track water-column redox conditions, we integrate organic geochemical (biomarker) data, iron-based redox-proxies, redox-sensitive trace elements, pyrite sulfur isotope values, and total organic carbon contents. As previous studies have suggested an empirical relationship between subsurface anoxia and the distribution of eukaryotic microfossils (Javaux et al., 2001; Shen et al., 2003; see also Butterfield and Chandler, 1992), we also document the composition of microfossils preserved in basinal Arlan shales. These data are then placed in the context of information from other basins to examine redox heterogeneity in Mesoproterozoic oceans.

GEOLOGIC BACKGROUND

Geology of the Ural Mountains and Volgo-Ural region

For many years, Russian geologists discussed Meso- and early Neoproterozoic stratigraphy in terms of a Riphean stratotype located in the Bashkirian meganticlinorium, a large structure on the western slope of the southern Ural Mountains (Chumakov and Semikhatov, 1981; Keller and Chumakov, 1983). In the southern Urals, the lower Mesoproterozoic (Lower Riphean) is represented by the Burzyan Group, traditionally divided into the Ai, Satka and Bakal formations in ascending stratigraphic order (Fig. 1B). The age of Burzyan deposition is constrained by the ~1380 Ma Mashak volcanics in the overlying Middle Riphean Yurmata Group (Puchkov et al., 2013; Krasnobaev et al.,

2013a) and ~1750 Ma basalts 200 meters above the base of the Ai Formation (Puchkov et al., 2012, Krasnobaev et al., 2013b) (Fig. 1B).

In the Volgo-Ural region to the west, sub-surface Riphean stratigraphy is known from core and geophysical data. The Kyrpy Group in this region, correlated to Lower Riphean deposits of the Bashkirian meganticlinoriun, consists of the Kaltasy, Nadezhdino and Kabakovo formations. The Kyrpy Group previously included the Nadezhdino Formation as well (see Kah et al., 2007, their Fig. 2), but this formation was recently transferred to the overlying Serafimovka Group (Kozlov et al., 2009). The Kaltasy Formation, of interest here, is correlated with the Satka Formation in the Ural Mountains (Keller and Chumakov, 1983; Kah et al., 2007; Kozlov et al., 2009) and is subdivided into the conformable Sauzovo (not recognized in this core; Kozlov et al., 2011), Arlan and Ashit members. The formation ranges in thickness from 1230 to 3600 m. The Arlan Member (535 to 1216 m thick) is represented by carbonaceous shales (some of them fossiliferous) and subordinate siltstones, dolostones, limestones and dolomitic marls.

Depositional environment of the Arlan Member in the 203 Bedryazh core

Redox profiles of paleo-basins are most easily interpreted through transects of multiple stratigraphic sections in a sequence stratigraphic context (e.g. Shen et al., 2003; Poulton et al., 2010; Sperling et al., 2013). A sequence stratigraphic framework for the Kyrpy Group has not been established, and core coverage across this basin was not available; consequently, interpretation of redox chemistry in relation to paleo-water depth must be determined with respect to sedimentological indicators in the studied strata themselves. Such an approach has proven useful in many recent studies of Proterozoic

sedimentary geochemistry (e.g., Johnston et al., 2010; 2012; Cumming et al., 2013; Wilson et al., 2010).

In the 203 Bedryazh core, the Arlan Member consists almost entirely of parallel laminated dark shales with minor, commonly diagenetic micrite/dolomicrite. No wave- or current-generated sedimentary structures are present, suggesting persistent deposition below storm wave-base. Although some shallow environments may exhibit laminations and a lack of wave-generated sedimentary structures (for instance isolated lagoons), such conditions only exist on relatively short stratigraphic scales. The complete uninterrupted absence of wave activity for over a kilometer of stratigraphic thickness strongly argues these sediments were deposited beneath wave base, and further, far enough below wave base that any sea-level oscillations did not bring the environment within the reach of storm waves. Consistent with this view, Kah et al. (2007) argue that the 203 Bedryazh drillcore penetrates some of deepest Arlan facies found in the entire basin.

The perennial question in pre-Mesozoic paleoceanography concerns the water-depth of sediments deposited beneath storm wave-base -- these 'deep' or 'basinal' strata are almost certainly not 'deep' in the oceanographic sense of an average ocean depth of four kilometers. While the only hard constraint on these strata is that they were deposited in water depths persistently greater than ~150 meters (as indicated by the lack of wave-generated sedimentary structures), such strata are generally considered more likely to fall into the depth range of several hundred meters rather than being significantly deeper. From a comparative sedimentological standpoint, the Arlan Member investigated here is closely comparable to 'basinal' strata recognized in stratigraphic studies of other Proterozoic basins, such as the Roper Group (Abbott and Sweet, 2000; Shen et al., 2003)

or Fifteenmile Group (Sperling et al., 2013). The Arlan here is distinct from 'outer shelf' strata in those studies, which contain thin intercalated sandstones with sedimentological structures such as hummocky cross-stratification (Abbott and Sweet, 2000), indicating shallower conditions in the presence of storm waves.

MATERIALS AND METHODS

Re-Os geochemistry

For Re-Os geochronology, samples were collected from two intervals of the 203 Bedryazh drill core; a) 4197.97 m to 4198.50 m and b) from 4297.05 m to 4297.40 m (arrows on Fig. 1C stratigraphic column). These intervals were analyzed following methodology in Selby and Creaser (2003), Cumming et al. (2013), and references therein. Briefly, samples were digested and equilibrated in $Cr^{VI}O_3$-H_2SO_4 together with a mixed tracer (spike) solution, and Re and Os were extracted and purified using solvent extraction, micro-distillation, anion column chromatography methods and negative ion mass spectrometry. Isotopic measurements were performed using a ThermoElectron TRITON mass spectrometer. Full materials and methods and precision estimates for all geochemical analyses are located in Supporting Information.

Iron, carbon, sulfur and major/minor element geochemistry

The core was sampled as closely as possible based on existing core coverage (Fig. 1C). Samples were first analyzed for iron speciation chemistry. Three pools of highly-reactive iron (iron carbonate, iron oxides, and magnetite) were quantified using standard sequential-extraction protocols (Poulton and Canfield, 2005). Pyrite iron was determined

using a hot chromous chloride extraction (CRS) and gravimetric quantification as Ag_2S (Canfield et al., 1986). In addition to these four pools normally measured in studies of iron partitioning, a subset of samples (Table S2) were analyzed for other iron phases that could affect interpretation of iron speciation. Specifically, iron associated with Acid Volatile Sulfide (AVS) was quantified using the hot 6N HCl + $SnCl_2$ extraction of Rice et al. (1993), and iron in Poorly Reactive Silicates (Fe_{PRS}) was quantified with a 1-minute boiling HCl extraction and calculated as the difference between that value and the sum of the sequentially-extracted phases (Cumming et al., 2013). Pyrite sulfur isotope values were determined on the silver sulfide from the CRS extraction via combustion in a Costech Elemental Analyzer linked to a Thermo Scientific Delta V mass spectrometer in continuous flow mode (measured as SO-SO_2). Major, minor and trace elements (with the exception of Re and Os), were measured via ICP-AES at SGS Laboratories, Canada, following a standard four-acid digestion. Percent carbonate carbon was determined by mass loss following acid dissolution, and percent organic carbon was quantified by combusting acidified samples within a Carlo Erba NA 1500 Elemental Analyzer attached to a Thermo Scientific Delta V Advantage mass spectrometer.

Organic geochemistry and paleobiology

The Bedryazh-203 core was drilled with water-based fluids, not oil-based lubricants, and so was considered potentially suitable for an analysis of the lipid biomarkers associated with the rocks. For biomarker analysis and preparation, three samples (*b* on Fig. 3 stratigraphic column) from the core were selected. An organic geochemical preparation procedure (see Supporting Information) was used on these

samples, beginning with a number of steps to remove external contamination, including removing the outside edges, followed by crushing using a cleaned puck mill, and extraction with a mixture of organic solvents in a high-pressure, high-temperature cell. Finally, the bitumen extract was analyzed using gas chromatography and mass spectrometry to identify lipid biomarkers.

Samples taken throughout the core were processed for microfossils using standard palynological methods (e.g., Sergeev et al., 2011). Full materials, methods and precision estimates for all analyses are given in Supporting Information.

RESULTS

Re-Os geochemistry

Elemental Re and Os abundances for horizon 4198 m range from 0.1 to 0.6 ppb, and 11.3 to 34.6 ppt, respectively, with $^{187}Re/^{188}Os$ and $^{187}Os/^{188}Os$ ratios between 42 and 109, and 1.204 and 2.795, respectively (Table S3). The samples from the 4297 m interval have Re abundances from 0.1 to 0.7 ppb and Os abundances from 10.3 to 32.8 ppt. Isotopic ratios for $^{187}Re/^{188}Os$ and $^{187}Os/^{188}Os$ range from 60 to 138 and from 1.558 to 3.652, respectively; Table S2). Regression of the isotopic composition data for the 4198 m interval yields a Model 1 age of 1414 ± 40 Ma (n = 6, Mean Square of Weighted Deviates [MSWD] = 0.35, initial $^{187}Os/^{188}Os$ [Os_i] = 0.20 ± 0.06; Fig. 2A). The Re-Os isotopic data for the 4297 m interval yields a Model 1 age of 1427 ± 43 Ma (n = 6, [MSWD] = 0.23, initial $^{187}Os/^{188}Os$ [Os_i] = 0.12 ± 0.09; Fig. 2B).

Redox-proxy geochemistry

Iron speciation chemistry focuses on the ratio of operationally defined 'highly-reactive' iron pools (FeHR = iron in pyrite plus iron reactive to sulfide on early diagenetic timescales—namely iron carbonates and iron oxides, including magnetite) to total iron (FeT) in fine-grained siliciclastic sedimentary rocks. In these samples, reactive iron is dominated by iron carbonate (51%), followed by iron in pyrite (22.5%), iron oxide (13.5%) and magnetite (13%). No significant acid-volatile sulfide was detected in the samples analyzed (Table S2 and Supporting Information). Iron in poorly-reactive silicates (Fe_{PRS}) averaged 1.70 ± 0.45 wt% (Table S2 and Supporting Information) and while some samples showed enrichment, most are not significantly enriched compared to many Phanerozoic shales (Poulton and Raiswell, 2002; Cumming et al., 2013; see also Supporting Information). FeHr/FeT is relatively constant throughout the Arlan Member (FeHr/FeT = 0.14 ± 0.04: Fig. 3). Both total iron (3.26 ± 0.61 wt%) and total aluminum (7.36 ± 1.44 wt%) are slightly less than average shale composition (4.43 and 8.94 wt%, respectively; Gromet et al., 1984), with an average Fe/Al of 0.45 ± 0.06 (Fig. 3). Arlan shales are calcareous (24 ± 10%), perhaps leading to lower FeT and Al via dilution. Total organic carbon contents are low for basinal shales, averaging 0.11 ± 0.08 wt% (Fig. 3), with modestly enriched pyrite sulfur isotope values (Fig. 3; $\delta^{34}S$ average = +13.2 ± 5.9 ‰). Redox-sensitive trace elements in Arlan samples are not enriched with respect to average shale (Gromet et al., 1984; Turekian and Wedehpol, 1961). This holds whether total abundances are considered, or if abundances are normalized to biogeochemically-conservative elements such as aluminum. For example, molybdenum and vanadium contents are only ~20% and 60% those found in average shale, respectively (0.56 ± 0.98 ppm and 76 ± 19 ppm).

Organic geochemistry

Organic geochemical data for analyzed samples are shown in Table 1. Two biomarker ratios for maturity, the 22S/(22S+22R) ratio of the C_{31} hopane and the ratio of C_{27} 17α-trisnorhopane (Tm) to C_{27} 18α-trisnorhopane (Ts), are commonly used to evaluate the burial depth and maturity of sedimentary organic material by reflecting isomerizations in the compounds that reach a stable end point during hydrocarbon generation (Moldowan et al. 1986; Peters et al. 2005). The range in these proxies across the 203 Bedryazh samples is small, showing a uniformly mature organic content in these samples and suggesting that there has been no later input of less-mature hydrocarbons to the lipid pool.

In basins where sedimentary organic matter is of appropriate maturity and does not show later contamination, hydrocarbon biomarkers can provide a means of reconstructing paleoenvironmental conditions independent of lithology (Brocks and Summons, 2003; Peters et al., 2005). The ratio of C_{26}/C_{25} tricyclic terpanes to C_{31}/C_{30} hopanes can be used to differentiate marine from lacustrine source rocks, as these compounds are produced in different ratios by microorganisms from these environments (Peters et al. 2005). Similarly, the ratios of C_{24}/C_{23} tricyclic terpanes and C_{22}/C_{21} tricyclic terpanes vary among depositional environments. (Zumberge 1987; Peters et al. 2005). In the 203 Bedryazh core samples, these proxies are consistent with shale deposition in a marine setting (Table 1).

The biomarker proxies that reflect redox conditions indicate generally oxic conditions (Table 1). These include 1) low ratios of longer chain homohopanes – hopanes

derived from polyfunctional C_{35} hopanoids present in bacteria; 2) low concentrations of 28,30 bisnorhopane; and 3) absence of the biomarkers of the photosynthetic sulfur bacteria Chlorobi (Peters et al., 2005; Summons and Powell, 1986).

Paleobiology

Microfossils occur throughout the sampled interval of the core. The Arlan Member assemblage is dominated by large (commonly > 100 μm) spheroidal fossils, along with subordinate filaments (Fig. 4). Specifically, the assemblage comprises the remains of relatively large and morphologically complex forms including such taxa as *Leiosphaeridia*, *Synsphaeridium, Polytrichoides, Brevitrichoides, ?Chuaria, Siphonophycus, Oscillatoriopsis* and others. These microfossils are likely the remains of both cyanobacteria and eukaryotic microorganisms. The eukaryotic affinity of at least some of these forms is supported by evidence of the occupation of a spheroidal envelope by a single large cell (e.g., Fig. 4.10), thick walls, and/or ornamentation in the form of pleats (Fig. 4.4) and possible processes (Fig. 4.6). We thus interpret the Arlan assemblage as a predominantly prokaryotic (cyanobacterial) microbiota that contains a modest diversity of eukaryotic organisms that lived in the surface waters in a basinal setting.

DISCUSSION

Re-Os ages and Os_i through time

Although the ages obtained are relatively imprecise (± 3%) due to the limited range in $^{187}Re/^{188}Os$ and $^{187}Os/^{188}Os$, they are consistent with existing geochronological

constraints for Lower Riphean strata from the southern Ural Mountain outcrop belt. Specifically, the ages of 1414 ± 40 Ma and 1427 ± 43 Ma for the Lower Riphean in the Kyrpy Group are consistent with the bracketing ages on the Lower Riphean in the southern Urals from the ~1380 Ma Mashak volcanics and the ~1750 Ma Ai basalts (Puchkov et al., 2012; 2013; Krasnobaev et al., 2013 a,b). Equally important, geochronology indicates that Arlan deposition was broadly synchronous with those of successions in Australia and North America that have been foci of previous investigations of mid-Proterozoic redox profiles.

Existing initial Os isotope data from the Archean to the early Phanerozoic suggest that the seawater Os isotope composition evolved from mantle-like values being sourced predominantly from mantle-derived rocks via hydrothermal input to a crust-dominated (isotopically evolved units) weathering influx during the Mesoproterozoic (Fig. 2C). This transition has been interpreted as the onset of weathering of continental crust in a newly oxidized environment (van Acken et al. 2013 and references therein). Our new initial Os isotope data do not contradict this observation, but we note there is a paucity of data (<30 Os_i values for 3 Gy of Earth history), of which some possess significant uncertainties (~≤ ±0.3 $^{187}Os/^{188}Os$ units). Thus until more precise Os_i data is available we advise caution when evaluating paleoenvironmental conditions using only Os isotopes.

Redox state of the Arlan Member, 203 Bedryazh core

The iron speciation proxy has been well-calibrated in modern oxic and anoxic depositional settings: sediments deposited beneath an oxic water column generally have an FeHR/FeT ratio < 0.38 (Raiswell and Canfield, 1998), while sediments from anoxic

basins are enriched in highly-reactive iron (FeHR/FeT > 0.38). The entire Arlan Member falls firmly within the range conventionally interpreted as 'oxic,' with only one sample falling above the modern oxic average of 0.26 (but still below 0.38; Raiswell and Canfield, 1998) (Fig. 3). As noted above, the Arlan Member is relatively calcareous; however, this is unlikely to dramatically affect our interpretation, for two specific reasons. Foremost, the modern calibration dataset covers the range of carbonate contents preserved in the Arlan Member (Raiswell and Canfield, 1998). Further, the primary effect of carbonate addition on iron speciation should be to add ferrous iron during diagenesis, and this would bias the Arlan samples towards an anoxic signal. Certain sedimentological regimes can also influence Fe-speciation data (for example, rapid sedimentation: see Raiswell and Canfield, 1998; Lyons and Severmann, 2006; Poulton and Canfield, 2011; and Farrell et al., 2013, for discussion of caveats regarding iron-based redox proxies); however, no evidence for such conditions is preserved within the 203 Bedryazh core.

It has recently been recognized in iron speciation studies that under anoxic and ferruginous water columns, authigenic iron-rich clays may precipitate (e.g. Cumming et al., 2013). The exact conditions causing such precipitation are still unknown, but as the iron in these authigenic clays are not extracted by the sequential extraction protocol employed here (Poulton and Canfield, 2005), such enrichments will be missed, and an anoxic water-column might appear 'oxic.' The presence of iron-rich clays can be tested in two ways using bulk geochemical methods. First, iron in poorly-reactive silicates (Fe_{PRS}) will be extracted by a 1-minute boiling HCl extraction, and so significant Fe_{PRS} will indicate authigenic clay enrichment (Cumming et al., 2013). Most Arlan member shales investigated do not show significant Fe_{PRS} enrichments (Table S2 and Supporting

Information). Second, total iron enrichments can be tested with the Fe/Al ratio (Lyons and Severmann, 2006). Aluminum is present primarily in the detrital phase, thus allowing the recognition of authigenic iron enrichment in *any* phase, while also serving to normalize dilution by carbonate. The Fe/Al values from the Arlan Member fall at or below values for average shale (Gromet et al., 1984; Turekian and Wedehpol, 1961), implying no enrichment of total iron and, by extension, no anoxia.

The other redox indicators investigated here also support an oxygenated Mesoproterozoic water-column, or, at the least, provide no evidence for anoxia. Sulfur isotopes provide an independent window into paleoenvironmental conditions. Though Early Mesoproterozoic sulfate records are thin, published values for sulfate from the ~1400-1500 Ma Belt Supergroup, Montana, USA, show relatively large stratigraphic variation, with a mean $\delta^{34}S$ composition of 15.0 ± 5.8 ‰ (Gellatly and Lyons, 2005). In this context, the average pyrite sulfur isotope values in our Arlan samples ($\delta^{34}S$ = 13.2 ± 5.9‰) are essentially the same as sulfate values from coeval Belt rocks, implying that seawater sulfate was near-quantitatively reduced in the Arlan sediments. This points to diffusion limitation of the sulfate supply, most simply achieved when oxygen in overlying seawater drives the sulfate reduction zone into the sediment column. We note, however, that this isotopic pattern only demands a limited sulfate supply to the site of sulfate reduction; it could also be achieved under a ferruginous water column, or through extremely high levels of sulfate reduction and depletion of a small basinal sulfate reservoir (e.g. Shen et al., 2003).

Redox-sensitive trace elements, especially when interpreted in parallel, can give insight into water column redox conditions (Tribovillard et al., 2006). For example, Mo is

efficiently scavenged from seawater only in the presence of sulfide, whereas V enrichment can occur under less strongly reducing conditions (Tribovillard et al., 2006). When elemental abundances are analyzed from shales that have been independently determined to be anoxic, for instance with iron speciation data, these redox-sensitive trace elements can also provide insight into basinal hydrography and the global spread of reducing sinks (Algeo and Rowe, 2012; Reinhard et al., 2013). Neither Mo nor V are enriched in the Arlan shales (Fig. 3). Interpreted in the traditional framework where water-column anoxia leads to trace metal enrichment, this would suggest an oxic or at least non-euxinic water column for these Arlan shales. However, due to widespread reducing sinks, trace metal enrichments in anoxic sediments in the Proterozoic are generally muted (Reinhard et al., 2013), potentially limiting their usefulness as local water-column redox proxies during this time (Scott and Lyons, 2012). Certainly, though, Arlan Member trace element data do not provide evidence for anoxia.

Organic geochemical data from selected Arlan samples further reveal no evidence for anoxia. In contrast to coeval deposits of the MacArthur Basin, Australia (Brocks et al., 2005), Arlan samples contain no detectable carotenoid biomarkers (isorenieratane, chlorobactane and okenane) indicative of photic-zone euxinia. Although the absence of these biomarkers alone does not suggest an oxic depositional environment, and is also consistent with a ferruginous condition, evidence for an oxygenated environment is supported by the low abundances of C_{31}-C_{35} homohopanes and 28,30 bisnorhopane (Table 1) (Peters et al., 2005). As with any ancient rocks (and especially considering the low organic carbon contents of Arlan shales), the possibility of younger contamination exists (e.g. Rasmussen et al., 2008). However, other lipid biomarker ratios measured for

depositional environment and maturity suggest an autochthonous source for the organic compounds present. Further, any such contamination must have simultaneously 1) erased any primary evidence for anoxia while 2) failing to add any signature of inconsistent maturity, different depositional environments, or younger biological groups such as plants or animals, and thus the redox signal from organic geochemistry is most parsimoniously regarded as syngenetic.

Organic geochemical data from selected Arlan samples further reveal no evidence for anoxia. In contrast to coeval deposits of the MacArthur Basin, Australia (Brocks et al., 2005), Arlan samples contain no detectable carotenoid biomarkers (isorenieratane, chlorobactane and okenane) indicative of photic-zone euxinia. Although the absence of these biomarkers alone does not suggest an oxic depositional environment, and is also consistent with a ferruginous condition, evidence for an oxygenated environment is supported by the low abundances of C_{31}-C_{35} homohopanes and 28,30 bisnorhopane (Table 1) (Peters et al., 2005). As with any ancient rocks (and especially considering the low organic carbon contents of Arlan shales), the possibility of younger contamination exists (e.g. Rasmussen et al., 2008). However, other lipid biomarker ratios measured for depositional environment and maturity suggest an autochthonous source for the organic compounds present. Further, any such contamination must have simultaneously 1) erased any primary evidence for anoxia while 2) failing to add any signature of younger biological groups such as plants or animals, and thus the redox signal from organic geochemistry is most parsimoniously regarded as syngenetic and recording an oxic water column.

The final piece of evidence regarding redox state comes from the eukaryotic microfossil record. As early as 1990, Vidal and Nystuen (1990) noted that in Proterozoic successions, basinal deposits generally lack the eukaryotic microfossils commonly found in younger successions. Butterfield and Chandler (1992) developed this theme further, stating that unambiguously eukaryotic fossils are absent from deep basinal facies in most Proterozoic successions. Javaux et al. (2001) tested this hypothesis in the ~1500-1400 Roper Group, Australia, documenting the distribution of microfossils across a depth gradient recorded by multiple stacked sedimentary sequences. Indeed, in Roper successions, taxa interpreted as eukaryotic occur only or most abundantly in shore-face to storm-dominated shelf deposits; microfossils likely to be eukaryotic are rare in basinal shales.

Given the sensitivity of most eukaryotic organisms to anoxic environments, such a distribution can be explained in terms of the probability that organisms in oxic surface waters would be challenged by upward-mixing anoxic water masses. In most basins that probability was low in nearshore environments in direct contact with the atmosphere through wave and wind mixing, but high in basinal settings. A corollary of this hypothesis is that eukaryotes should show a wider distribution across facies in basins characterized by oxic subsurface waters, and that is what we observe in the Arlan samples.

In summary, iron geochemical data and the paleobiological record paint a consistent picture of life and environments and provide evidence from two independent data sources that Arlan shales recovered from the 203 Bedryazh borehole were deposited under an oxygenated water column. Redox-sensitive trace elements, pyrite sulfur isotope

values, and biomarker data are consistent with an oxic water column, but as discussed above, caveats exist. Indeed, it is recognized that unlike the detection of euxinia in the ancient record, for which the iron, sulfur, trace element (particularly Mo) and organic geochemical records provide independent tests (Lyons et al., 2009), there are few independent geochemical metrics distinguishing oxic from ferruginous conditions. As it is increasingly recognized that ferruginous water columns may have been the dominant anoxic state for long periods of Earth history (Poulton and Canfield, 2011), the development of independent tests to complement iron-based proxies would have high utility. Alternatively, as discussed here, geochemical data can be coupled with paleobiological observations to provide such an independent measure of oxic/anoxic conditions.

Mesoproterozoic redox heterogeneity in a global context

The Re-Os ages obtained here indicate that deposition of oxygenated basinal Arlan shales broadly overlapped temporally with euxinic and ferruginous conditions in the Roper (Shen et al., 2003) and Belt (Planavsky et al., 2011) basins. The almost inescapable conclusion is that just as oxygen concentrations in the modern ocean are heterogeneous (Helly and Levin, 2004), oxygen concentrations at depth in the Mesoproterozoic ocean were spatially variable as well. Surface waters in Proterozoic oceans were almost undeniably oxygenated after 2.4 Ga (Shen et al., 2003; Canfield et al., 2008; Sperling et al., 2013), so the question rests with the nature of deeper-water chemistry and the drivers underpinning observed spatial heterogeneity.

The oxygen content of subsurface marine waters is determined by the initial loading of O_2 into downwelling water masses, the ventilation time of deep waters, and the rate of organic carbon export from the surface mixed layer (Sarmiento et al., 1988). Even today, when surface waters are in equilibrium with an atmosphere containing 21% O_2, dysoxic to anoxic regions occur across large swaths of the Pacific, Indian, and eastern tropical to subtropical Atlantic oceans (Helly and Levin, 2004). Moreover, studies of current global warming show that as ocean temperatures rise, oxygen minimum zones are both shoaling and expanding laterally, driven by T-dependent changes in saturation and perhaps by increased stratification of surficial water masses (Keeling et al., 2010; Gilly et al., 2013). In a mid-Proterozoic ocean, with much lower atmospheric pO_2 and warm seawater temperatures (decreasing oxygen content, enhancing water column stratification, and increasing rates of bacterial respiration, e.g., Ulloa et al., 2012; Gaidos and Knoll 2012), widespread oxygen depletion beneath surface waters might in fact be predicted. Given these controls, how does one account for oxic basinal water masses indicated by the Arlan shales?

Possibly, the oxygen minimum zone was simply at depths greater than those recorded by the Arlan deposits – in the modern ocean, the OMZ may lie hundreds of meters or more beneath the sea surface (Gilly et al. 2013). Studies of other mid-Proterozoic basins, though, record oxygen depletions bathing the bottoms of shelf and platformal seas in environments similar to that of the Arlan. It is worth emphasizing again that none of the Proterozoic basins being discussed represent true 'deep ocean,' but rather moderate depths beneath storm wave-base. Thus while the redox state of the deep ocean remains an open question (but see Slack et al., 2007; 2009), the differences

between the oxygenated Kyrpy Group, ferruginous Belt Supergroup, and euxinic Roper Group, whose basinal deposits represent broadly similar environments, requires explanation. Tectonics is unlikely to provide an answer, as the Lower Riphean basin of the Uralian region was either a shelf/platform setting much like those observed elsewhere or a rift basin (Puchkov, 2013), which would tend to enhance the prospect of restriction and subsurface anoxia.

Alternatively, Holland (2006) calculated that even at atmospheric oxygen levels of 10% of the modern, oxygenated conditions at depth are possible if organic carbon delivery is low. The redox data from the Mesoproterozoic Arlan Member is interpreted here as the geochemical manifestation of Holland's prediction, showing the persistence of oxic conditions in a region of low export production, recorded by the unusually low TOC in Arlan shales. We interpret the Arlan basin as oligotrophic with correspondingly low delivery rates of organic matter to subsurface water masses.

CONCLUSIONS

All redox proxies from the Arlan Member indicate that deposition occurred beneath an oxygenated water column. These data cannot inform the absolute concentration of O_2 either dissolved in seawater or present in the atmosphere; however, they do inform the mechanisms that controlled subsurface water chemistry in Mesoproterozoic oceans. It is worth emphasizing that these data are not interpreted as a mid-Proterozoic 'oxygenation event'—rather, they demonstrate that sub-surface waters in at least one basin were oxygenated at a time when most basins appear have sustained anoxic water masses at depth. Because there were local as well as global controls on

marine redox profiles, no single stratigraphic section or basin can serve as exemplar for the entire ocean at a given time point. In conjunction with global isotopic redox tracers, the evaluation of the redox state in multiple sections/basins worldwide, analyzed in a statistical framework, will ultimately be needed to distinguish global signals from local heterogeneity. That said, previous data and the results reported here collectively paint an increasingly nuanced picture of mid-Proterozoic oceans that includes moderately oxic surface waters; underlying oxygen minimum zones that were weakly oxic, ferruginous, or euxinic, depending on organic carbon loading and, perhaps, nitrogen chemistry (Boyle et al., 2013); and dysoxic water masses in the deep ocean (Slack et al., 2007, 2009). Such geographic and bathymetric heterogeneity provides a necessary framework for interpreting phenomena that range from the "boring billion" stasis in C-isotopic records (Buick et al., 1995) to the persistence of low pO_2 in the Proterozoic atmosphere (Johnston et al., 2009) and the early evolution of eukaryotic cells (Knoll et al., 2006).

ACKNOWLEDGEMENTS

We thank Ann Pearson and David Evans for helpful discussion, and Erin Beirne, Alex Morgan, Picov Andropov, Dan Schrag, Greg Eischeid, Andy Masterson for assistance in the field and in the lab. XXX was funded by Agouron Geobiology and NASA Astrobiology Institute Postdoctoral fellowships. This paper is dedicated to the late Dr. V.I. Kozlov, who kindly introduced XXX and XXX to the Precambrian stratigraphy of the Urals and helped facilitate our fieldwork.

FIGURE CAPTIONS

Fig. 1- A) Map of the southern Ural Mountains and Volgo-Ural region showing the location of the 203 Bedryazh borehole (filled circle) and Riphean stratotypes in the southern Ural Mountains. B) Generalized stratigraphic column of the Mesoproterozoic (Lower Riphean) deposits of the southern Ural Mountains (after Keller and Chumakov, 1983; Sergeev, 2006). Formation abbreviations: (Ai) Ai; (St) Satka; (Bk) Bakal; (Mh) Mashak. Other abbreviations: (PP) Paleoproterozoic; (LP) Lower Proterozoic; (MR) Middle Riphean; (Yur) Yurmanta Group; (ISC) International Stratigraphic Chart. Asterisks mark geochronological constraints for the Lower Riphean (Puchkov et al. 2012; 2013; Krasnobaev et al., 2013 a,b). Symbols denoting rock types are (1) limestone; (2) dolomite; (3) shale; (4) siltstone; (5) sandstone; (6) conglomerate; (7) tillite, tilloid; (8) bioherms with columnar stromatolites; (9) tuff, tuffaceous sandstone and diabase; (10) dolomite with chert lenses; (11) marl; (12) clay dolomites; (13) hiatus, unconformity; (14) azimuthal discordance; (15) basement gneiss. C) Generalized stratigraphic column of the Mesoproterozoic (Lower Riphean) and Ediacaran (Vendian) deposits of the 203 Bedryazh borehole (After Kah et al., 2007; Kozlov et al., 2009). Borehole depth in meters is given to the center of the column and available core is shown to right (dark lines). The most probable correlation of the Kaltasy Formation to the southern Ural Mountains Proterozoic succession is shown by dashed lines. New Re-Os age estimates from this core (this study) indicated by arrows. Abbreviation: (Ed) Ediacaran.

Fig. 2- Re-Os isochrons for the 203 Bedryazh shales. A) Depth range 4197.97 m to 4198.5 m. B) Depth range 4297.05 m to 4297.4 m. C) Evolution of seawater $^{187}Os/^{188}Os$ values from the Archean through to the early Phanerozoic. Adapted from van Acken et al. (2013), and updated with data from Bertoni et al. (in review), Geboy et al. (2013), Rooney et al. (2014) and Strauss et al. (in review). Open symbols: this study. Mantle Os isotope composition of 0.13 is from Meisel et al. (2001). The modern-day seawater Os isotope composition of 1.06 and the modern-day continental weathering flux of 1.4 (not shown) is from Peucker-Ehrenbrink and Ravizza (2000). Uncertainties in initial $^{187}Os/^{188}Os$ values are 2 sigma, uncertainties in ages are less than the size of the symbols.

Fig. 3- Redox proxy data for the Arlan Member (Kaltasy Formation) in the 203 Bedryazh borehole. Stratigraphic column after Kah et al. (2007) and Kozlov et al., (2009); note that while much of the column is depicted as carbonate, direct measurements of samples investigated (Table S2) indicates they are mainly calcareous shales. Locations of biomarker samples indicated by *b*. Redox proxies from left to right are 1) Ratio of highly-reactive (FeHR) to total iron (FeT); dashed line = 0.38. Blue shaded area to left of 0.38 ratio indicates samples likely deposited under an oxygenated water column. 2) Ratio of iron in pyrite (FeP) to FeHR; dashed line = 0.8, 3) Ratio of total iron (FeT) to total aluminum (Al); dashed line = average shale value of 0.5, 4) Molybdenum in ppm; dashed line = average shale value of 2.6 ppm; 5) Vanadium in ppm; dashed line = average shale value of 130 ppm; 6) Pyrite sulfur isotope values measured relative to Vienna Cañon Diablo Troilite standard and reported in per mil (‰) notation, 7) Total organic carbon contents reported in weight percent.

Fig. 4- Microfossils from the Arlan Member, 203 Bedryazh borehole. For all illustrated specimens, the sample number, its depth in meters in the 203 Bedryazh core (in parentheses), maceration slide number, and slide reference coordinates are provided. All specimens have been deposited to Paleontological Collection of the Geological Institute of Russian Academy of Sciences, collection # 14005. For all figures, the single bar is 50 μm and the double bar is 100 μm. 1, 1a (fragment of 1), *Leiosphaeridia jacutica*, 30 (4285 m) – 1 – 1. 2, *Leiosphaeridia atava* with multiple folds, 40 (3565 m) – 3 – 7. 3, *Synsphaeridium* sp., 39 (3944.5 m) – 3 – 5. 4, 4a (fragment of 4), *Leiosphaeridia* sp. with multiple folds, 34 (4169.7 m) – 6 – 3. 5, Envelope with problematic spines or pseudospines, 31 (4267 m) – 1 – 3. 6, 6a (fragment of 6), Ellipsoid of *Brevitrichoides bashkiricus* above the slim, 34 (4169.7 m) – 6 – 1. 8, Paired envelopes of *Leiosphaeridia atava,* 40 (3565 m) – 2 – 7a. 7, *Oscillatoriopsis longa*, 39 (3944.5 m) – 3 – 2. 9, Paired envelopes of *Leiosphaeridia jacutica,* 34 (4169.7 m) –3 – 2. 10, ?*Chuaria circularis*, 32 (4201.5 m) – 1 – 1. 11, *Pseudodendron* aff. *P. anteridium*, 40 (3565 m) – 3 – 1. 12, *Siphonophycus kestron* and *S. solidum*, 31 (4267 m) – 3 – 4. 13, *Rugosoopsis* sp., 34 (4169.7 m) – 7 – 1. 14, *Leiosphaeridia tenuissima* and *L. minutissima,* 40 (3565 m) – 3 – 5.

TABLES

Table 1- Organic geochemical (biomarker) ratios for investigated horizons in the 203 Bedryazh core.

REFERENCES

Abbott ST, Sweet IP (2000) Tectonic control on third-order sequences in a siliciclastic ramp-style basin: an example from the Roper Superbasin (Mesoproterozoic), northern Australia. *Australian Journal of Earth Sciences* **47**, 637–657.

Algeo TJ, Rowe H (2012) Paleoceanographic applications of trace-metal concentration data. *Chemical Geology* **324-325**, 6-18

Arnold GL, Anbar AD, Barling J, Lyons TW (2004) Molybdenum isotope evidence for widespread anoxia in mid-Proterozoic oceans. *Science* **304**: 87-90.

Bertoni ME, Rooney AD, Selby D, Alkmim FF, Le Heron DP, in review. Neoproterozoic Re-Os systematics of organic-rich rocks of the São Francisco Basin, Brazil and implications for hydrocarbon exploration. *Precambrian Research*.

Boyle RA, Clark JR, Poulton SW, Shields-Zhou G, Canfield DE, Lenton TM (2013) Nitrogen cycle feedbacks as a control on euxinia in the mid-Proterozoic ocean. *Nature Communications* **4**:1533.

Brocks JJ, Summons RE (2003) Sedimentary hydrocarbons, biomarkers for early life. In: *Treatise on Geochemistry* (eds. Holland HD, Turekian K). Pergamon, pp. 63–115.

Brocks JJ, Love GD, Summons RE, Knoll AH, Logan GA, Bowden SA (2005) Biomarker evidence for green and purple sulphur bacteria in a stratified Palaeoproterozoic sea. *Nature* **437**, 866-870.

Buick R, Des Marais D, Knoll AH (1995) Stable isotope compositions of carbonates from the Mesoproterozoic Bangemall Group, Australia: environmental variations, metamorphic effects and stratigraphic trends. *Chemical Geology* **123**, 153-172.

Butterfield NJ, Chandler, FW (1992) Paleoenvironmental distribution of Proterozoic microfossils, with an example from the Agu Bay Formation, Baffin Island. *Paleontology* **35**: 943-957.

Canfield DE (1998) A new model for Proterozoic ocean chemistry. *Nature* **396**, 450-453.

Canfield DE, Poulton SW, Knoll AH, Narbonne GM, Ross G, Goldberg T, Strauss H (2008) Ferruginous conditions dominated later Neoproterozoic deep-water chemistry. *Science* **321**, 949-952.

Canfield DE, Raiswell R, Westrich JT, Reaves CM, Berner RA (1986) The use of chromium reduction in the analysis of reduced inorganic sulfur in sediments and shales. *Chemical Geology* **54**, 149-155.

Chumakov NM, Semikhatov MA (2001) Riphean and Vendian of the USSR. *Precambrian Research* **15**, 229-253.

Cumming VM, Poulton SW, Rooney AD, Selby D (2013) Anoxia in the terrestrial environment during the late Mesoproterozoic. *Geology* **41**, 583-586.

Farrell UC, Briggs DEG, Hammarlund EU, Sperling EA, Gaines RR (2013) Paleoredox and pyritization of soft-bodied fossils in the Ordovician Frankfort Shale of New York. *American Journal of Science* **313**, 452-489.

Gaidos E, Knoll AH (2012) Our evolving planet: from the dark ages to an evolutionary renaissance. In: *Frontiers of Astrobiology* (eds. Impie C, Lunine J, Funes J). Cambridge University Press, pp. 132-153.

Geboy NJ, Kaufman AJ, Walker RJ, Misi A, de Oliviera TF, Miller KE, Azmy K, Kendall B, Poulton SW (2013) Re-Os age constraints and new observations of Proterozoic glacial deposits in the Vazante Group, Brazil. *Precambrian Research* **238**, 199-213.

Gellatly AM, Lyons TW (2005) Trace sulfate in mid-Proterozoic carbonates and the sulfur isotope record of biospheric evolution. *Geochimica et Cosmochimica Acta* **69**, 3813-3829.

Gilly WF, Beman JM, Litvin SY, Robison BH (2013) Oceanographic and biological effects of shoaling of the oxygen minimum zone. *Annual Review of Marine Science* **5**, 393-420.

Gromet LP, Dymek RF, Haskin LA, Korotev RL (1984) The "North American shale composite": Its compilation, major and trace element characteristics. *Geochimica et Cosmochimica Acta* **48**, 2469-2482.

Helly JJ, Levin LA (2004) Global distribution of naturally occurring marine hypoxia on continental margins. *Deep Sea Research Part I: Oceanographic Research Papers* **51**, 1159-1168.

Holland HD (1984) The chemical evolution of the atmosphere and oceans. Princeton University Press.

Holland HD (2006) The oxygenation of the atmosphere and oceans. *Philosophical Transactions of the Royal Society, London* **361B**, 903-915.

Javaux E, Knoll AH, Walter MR (2001) Ecological and morphological complexity in early eukaryotic ecosystems. *Nature* **41**, 66-69.

Johnston DT, Wolfe-Simon F, Pearson A, Knoll AH (2009) Anoxygenic photosynthesis modulated Proterozoic oxygen and sustained Earth's middle age. *Proceedings of the National Academy of Sciences, USA* **106**, 16925–16929.

Johnston DT, Poulton SW, Dehler CM, Porter S, Husson J, Canfield DE, Knoll AH (2010) An emerging picture of Neoproterozoic ocean chemistry: Insights from the Chuar Group, Grand Canyon, USA. *Earth and Planetary Science Letters* **290**, 64-73.

Johnston DT, Poulton SW, Goldberg T, Sergeev VN, Podkovyrov V, Vorob'eva NG, Bekker A, Knoll AH (2012) Late Ediacaran redox stability and metazoan evolution. *Earth and Planetary Science Letters* **335-336**, 25-35.

Kah LC, Bartley JK (2011) Protracted oxygenation of the Proterozoic biosphere. *International Geology Review* **53**, 1424-1442.

Kah LC, Crawford DC, Bartley JK, Kozlov VI, Sergeeva ND, Puchkov VN (2007) C- and Sr-isotope chemostratigraphy as a tool for verifying age of Riphean deposits in the Kama–Belaya Aulacogen, the East European Platform. *Stratigraphy and Geological Correlation* **15**, 12-29.

Keeling RF, Körtzinger A, Gruber N (2010) Ocean deoxygenation in a warming world. *Annual Review of Marine Science* **2**, 199-229.

Keller BM, Chumakov NM (Eds.) (1983) Stratotype of the Riphean, Stratigraphy, Geochronology. Nauka, Moscow, 184 p.

Kendall B, Creaser RA, Gordon GW, Anbar AD (2009) Re-Os and Mo isotope systematics of black shales from the Middle Proterozoic Velkerri and Wollogorang Formations, McArthur Basin, northern Australia. *Geochimica et Cosmochimica Acta* **73**, 2534-2558.

Knoll AH, Javaux EJ, Hewitt D, Cohen P (2006) Eukaryotic organisms in Proterozoic oceans. *Philosophical Transactions of the Royal Society, London* **361B**, 1023-1038.

Kozlov VI, Puchkov VN, Sergeeva ND (2011) New chart of geological succession revealed by the parametric borehole 1 Kulguninskaya. Institute of Geology, Ufa, 58 p.

Kozlov VI, Sergeeva ND, Mikhailov PN (2009) Stratgraphic subdivision of the boundary Upper Riphean, Vendian and Paleozoic deposits of western Bashkortosta. *Bulletin of the Regional Interdepartmental Stratigraphic Commission on the central and southern parts of the Russian Plate* **4**, 40-44 (In Russian)

Krasnobaev A, Kozlov VI, Puchkov VN, Busharina SV, Sergeeva ND, Paderin IP (2013a) Zircon Geochronology of the Mashak Volcanic Rocks and the Problem of the Age of the Lower–Middle Riphean Boundary (Southern Urals). *Stratigraphy and Geological Correlation* **21**, 465-481

Krasnobaev A, Puchkov VN, Kozlov VI, Sergeeva ND, Busharina SV, Lepekhina EN (2013b) Zirconology of Navysh Volcanic Rocks of the Ai Suite and the Problem of the Age of the Lower Riphean Boundary in the Southern Urals. *Doklady Earth Sciences* **448,** 185-190

Lyons TW, Anbar AD, Severmann S, Scott C, Gill BC (2009) Tracking euxinia in the ancient ocean: a multiproxy perspective and Proterozoic case study. *Annual Reviews Earth Planetary Sciences* **37**: 507-534.

Lyons TW, Severmann S (2006) A critical look at iron paleoredox proxies: New insights from modern euxinic marine basins. *Geochimica et Cosmochimica Acta* **70**, 5698-5722.

Meisel T, Walker RJ, Irving AJ, Lorand J-P (2001) Osmium isotopic compositions of mantle xenoliths: a global perspective. *Geochimica et Cosmochimica Acta* **65**, 1311-1323.

Moldowan JM, Sundararaman P, Schoell M (1986) Sensitivity of biomarker properties to depositional environment and/or source input in the Lower Toarcian of SW-Germany. *Organic Geochemistry* **10**, 915–926.

Partin CA, Bekker A, Planavsky NJ, Scott CT, Gill BC, Li C, Podkovyrov V, Maslov A, Konhauser KO, Lalonde SV, Love GD, Poulton SW, Lyons TW (2013) Large-scale fluctuations in Precambrian atmospheric and oceanic oxygen levels from the record of U in shales. *Earth Planetary Science Letters* **369-370**, 284-293.

Peters KE, Walters CC, Moldowan J (2005) The Biomarker Guide Second Edition, Cambridge University Press.

Peucker-Ehrenbrink B, Ravizza G (2000) The marine osmium isotope record. *Terra Nova* **12**, 205-219.

Planavsky NJ, McGoldrick P, Scott CT, Li C, Reinhard CT, Kelly AE, Chu X, Bekker A, Love GD, Lyons TW (2011) Widespread iron-rich conditions in the mid-Proterozoic ocean. *Nature* **477**, 448-451.

Poulton SW, Canfield DE (2005) Development of a sequential extraction procedure for iron: implications for iron partitioning in continentally derived particulates. *Chemical Geology* **214**, 209-221.

Poulton SW, Canfield DE (2011) Ferruginous conditions: A dominant feature of the ocean through Earth's history. *Elements* **7**, 107-112.

Poulton SW, Fralick PW, Canfield DE (2004) The transition to a sulphidic ocean ~1.84 billion years ago. *Nature* **431**, 173-177.

Poulton SW, Fralick PW, Canfield DE (2010) Spatial variability in oceanic redox structure 1.8 billion years ago. *Nature Geoscience* **3**, p. 486-490.

Puchkov VN, Krasnobnaev AA, Kozlov VI, Sergeeva ND (2012) New isotope ages of volcanics in the standard section of the Riphean and Vendian of the Southern Urals: consequences for stratigraphy and tectonics. In: *Materials for the IX-th Republican Conference on Geology and Environment*. Institute of Geology, Ufa, p. 52–56.

Puchkov VN, Bogdanova SV, Ernst RE, Kozlov VI, Krasnobaev AA, Soderlund U, Wingate MTD, Postnikov AV, Sergeeva ND (2013) The ca. 1380 Ma Mashak igneous event of the Southern Urals. *Lithos* **174**, 109-124.

Puchkov VN (2013) Structural stages and evolution of the Urals. Mineralogy and Petrology **106**, 3-37.

Rasmussen B, Fletcher IR, Brocks JJ, Kilburn MR (2008) Reassessing the first appearance of eukaryotes and cyanobacteria. *Nature* **455**, 1101-1104.

Raiswell R, Canfield DE (1998) Sources of iron for pyrite formation in marine sediments. *American Journal of Science* **298**, 219-245.

Reinhard CT, Planavsky NJ, Robbins LJ, Partin CA, Gill BC, Lalonde SV, Bekker A, Konhauser KO, Lyons TW (2013) Proterozoic ocean redox and biogeochemical stasis. *Proceedings of the National Academy of Sciences U.S.A.* **110**, 5357-62.

Rice CA, Tuttle ML, Reynolds RL (1993) The analysis of forms of sulfur in ancient sediments and sedimentary rocks: comments and cautions. *Chemical Geology* **107**, 83-95.

Rooney AD, Macdonald FA, Strauss JV, Dudás FÖ, Hallmann C, Selby D (2014) Re-Os geochronology and coupled Os-Sr isotope constraints on the Sturtian snowball Earth. *Proceedings of the National Academy of Sciences, USA* **111,** 51-56.

Scott C, Lyons TW (2012) Contrasting molybdenum cycling and isotopic properties in euxinic versus non-euxinic sedimentary rocks: refining the paleoproxies. *Chemical Geology* **324-325**, 19-27.

Selby D, Creaser RA (2003) Re-Os geochronology of organic rich sediments: an evaluation of organic matter analysis methods. *Chemical Geology* **200**, 225-240.

Sergeev VN (2006) Precambrian microfossils in cherts: their paleobiology, classification and biostratigraphic usefulness. GEOS, Moscow, 280 p. (In Russian)

Sergeev VN, Vorob'eva NG, Knoll AH (2011) Ediacaran microfossils from the Ura Formation, Baikal-Patom Uplift, Siberia: taxonomy and biostratigraphic significance. *Journal of Paleontology* **85**, 987-1011.

Sperling EA, Halverson GP, Knoll AH, Macdonald FA, Johnston DT (2013) A basin redox transect at the dawn of animal life. *Earth and Planetary Science Letters* **371-372**, 143-155.

Shen Y, Canfield DE, Knoll AH (2002) Middle Proterozoic ocean chemistry: evidence from the McArthur Basin, northern Australia. *American Journal of Science* **302**, 81-109.

Shen Y, Knoll AH, Walter MR (2003) Evidence for low sulphate and anoxia in a mid-Proterozoic marine basin. *Nature* **423**, 632-635.

Slack J, Grenne T, Bekker A, Rouxel O, Lindberg P (2007) Suboxic deep seawater in the late Paleoproterozoic: evidence from hematitic chert and iron formation related to seafloor-hydrothermal sulfide deposits, central Arizona, USA. *Earth and Planetary Science Letters* **255**, 243-256.

Slack JF, Grenne T, Bekker A (2009) Seafloor-hydrothermal Si-Fe-Mn exhalites in the Pecos greenstone belt, New Mexico, and the redox state of ca. 1720 Ma deep seawater. *Geosphere* **5**, 302-314.

Strauss JV, Rooney AD, Macdonald FA, Brandon AD, Knoll AH (in review) 740 Ma vase-shaped microfossils from the Yukon Territory: Implications for Neoproterozoic chronology and biostratigraphy. *Geology*.

Summons RE, Powell TG (1986) Chlorobiaceae in Palaeozoic seas revealed by biological markers, isotopes and geology. *Nature* **319**, 763–765.
Tribovillard N, Algeo TJ, Lyons T, Riboulleau A (2006) Trace metals as paleoredox and paleoproductivity proxies: an update. *Chemical Geology* **232**, 12-32.

Turekian KK, Wedepohl KH (1961) Distribution of the elements in some major units of the earth's crust. *Geological Society of America Bulletin* **72**, 175-192.

Ulloa O, Canfield DE, DeLong EF, Letelier RM, Stewart FJ (2012) Microbial oceanography of anoxic oxygen minimum zones. *Proceedings of the National Academy of Sciences, USA* 109,15996-16003.

Van Acken D, Thomson D, Rainbird RH, Creaser RA (2013) Constraining the depositional history of the Neoproterozoic Shaler Supergroup, Amunsden Basin, NW

Canada: Rhenium-osmium dating of black shales from the Wyniatt and Boot Inlet Formations. *Precambrian Research* **236**, 124-131.

Vidal G, Nystuen J (1990) Micropaleontology, depositional environment, and biostratigraphy of the upper Proterozoic Hedmark Group, Southern Norway. *American Journal of Science* **290-A**, 170-211.

Wilson JP, Fischer WW, Johnston DT, Knoll AH, Grotzinger JP, Walter MR, McNaughton, Simon M, Abelson J, Schrag DP, Summons R, Allwood A, Andres M, Gammon C, Garvin J, Rashby S, Schweizer M, Watters WA (2010) Geobiology of the Paleoproterozoic Duck Creek Formation, northwestern Australia. *Precambrian Research* **179**, 135-149.

Zumberge J (1987) Prediction of source rock characteristics based on terpane biomarkers in crude oils - a multivariate statistical approach. *Geochimica et Cosmochimica Acta* **51**, 1625–1637.

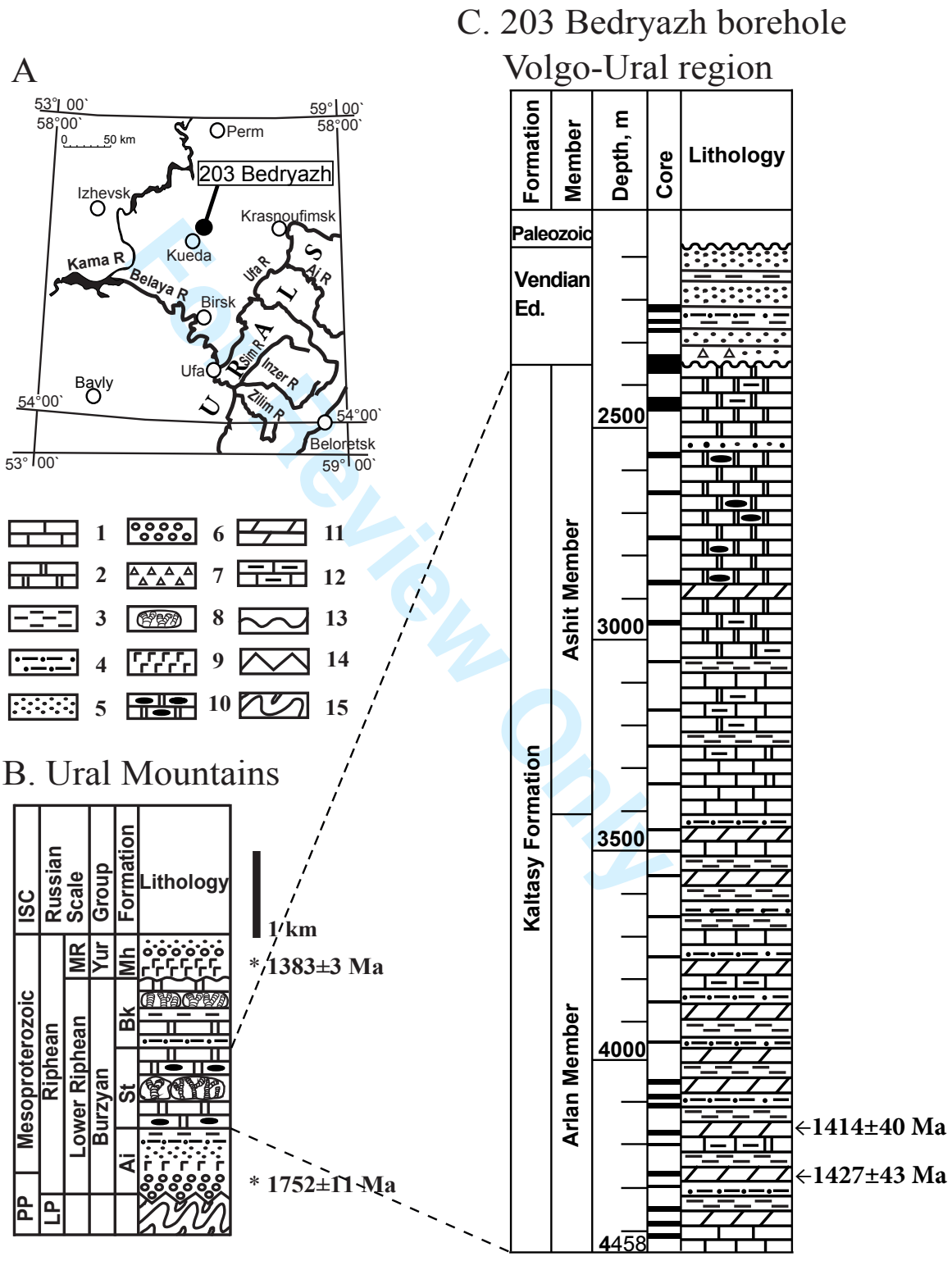

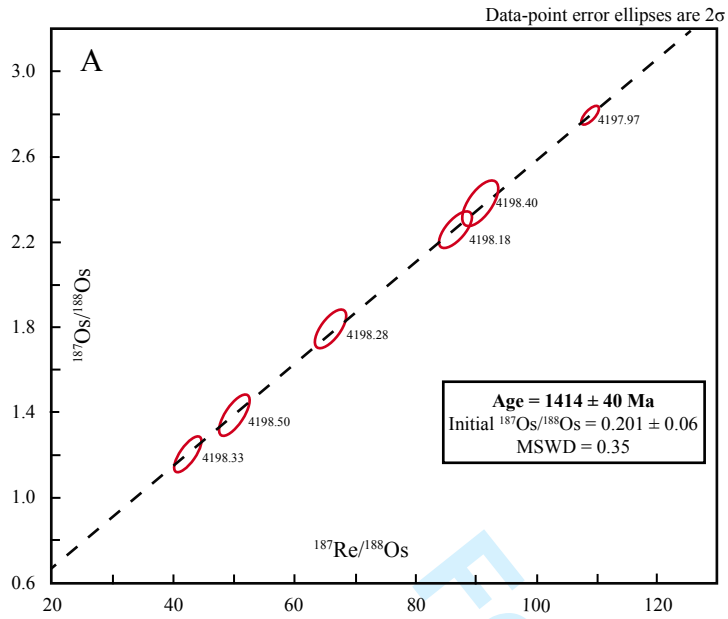

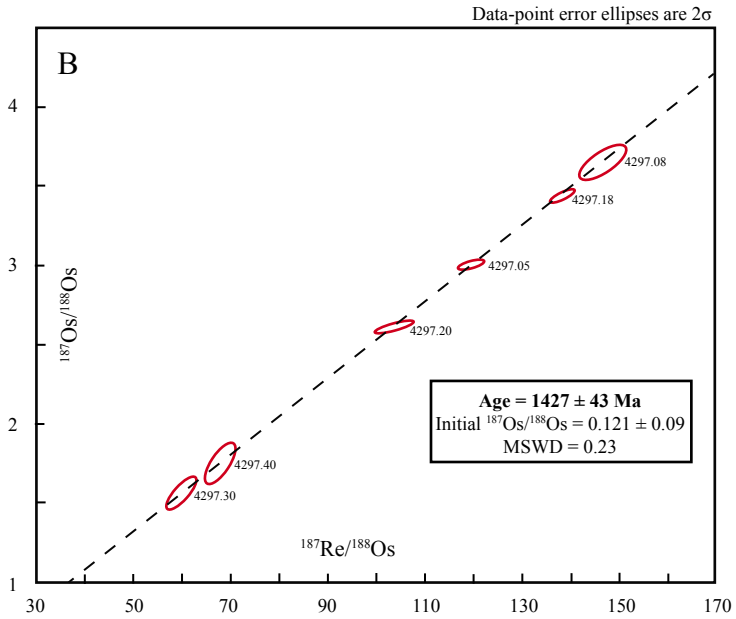

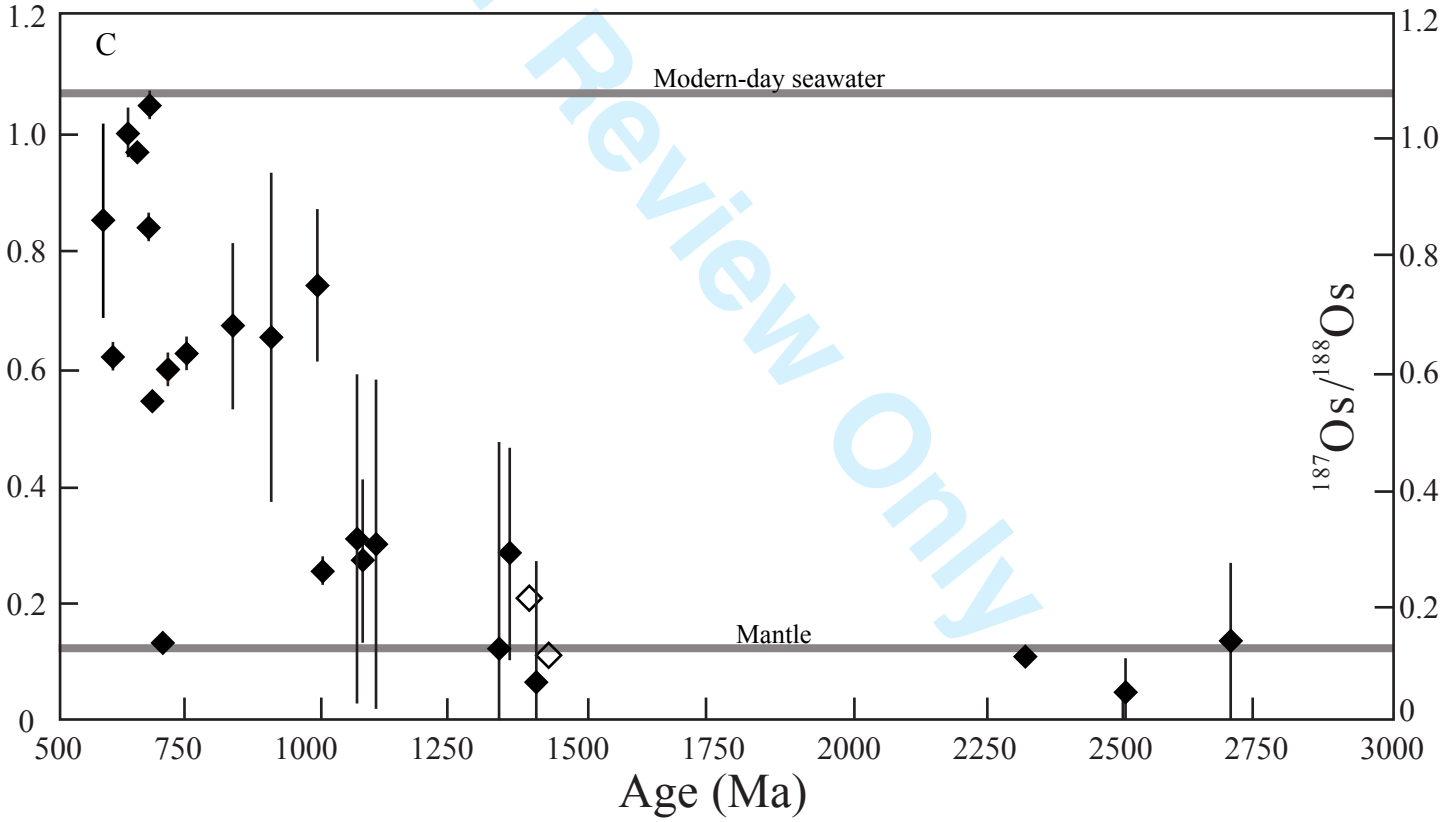

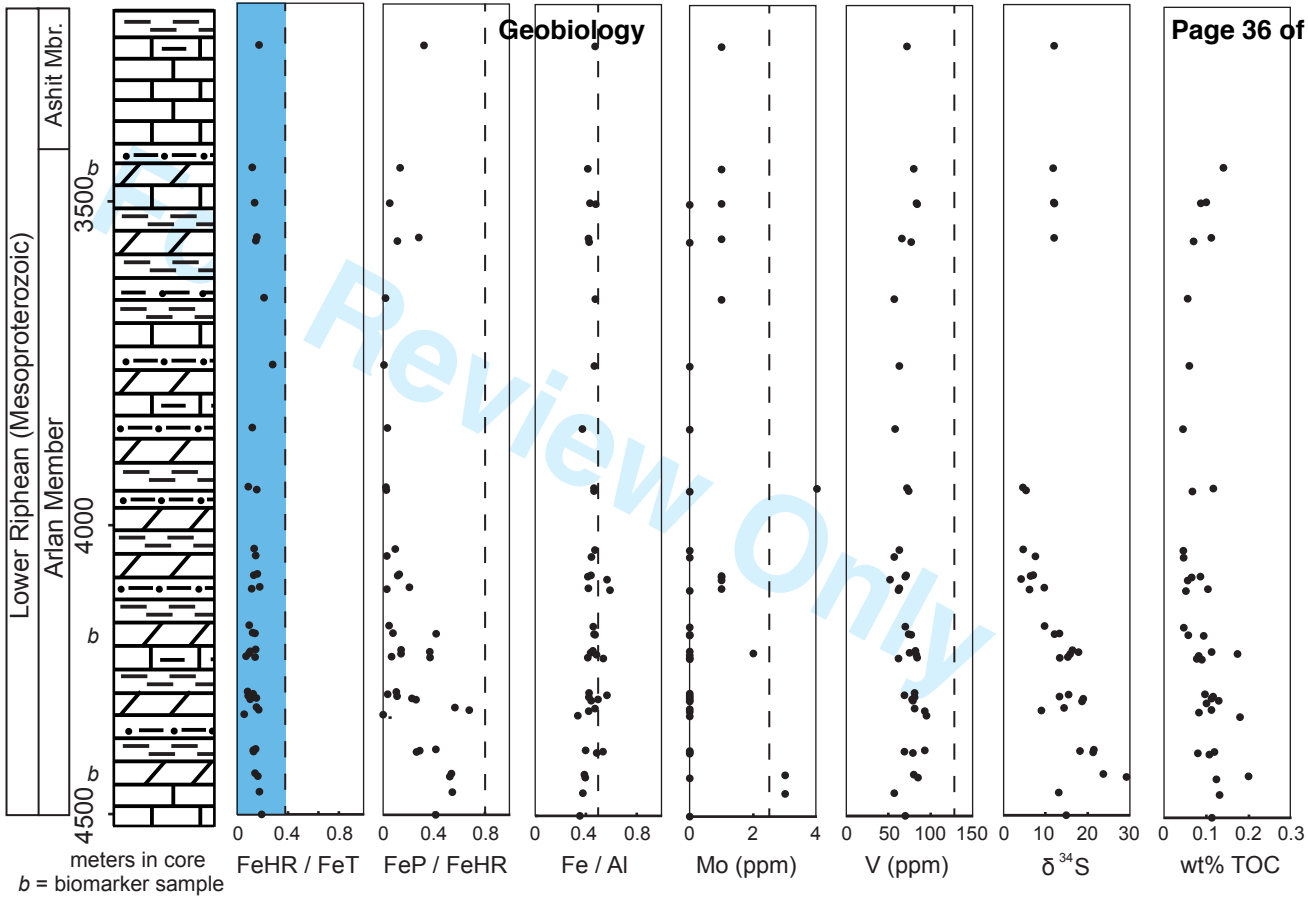

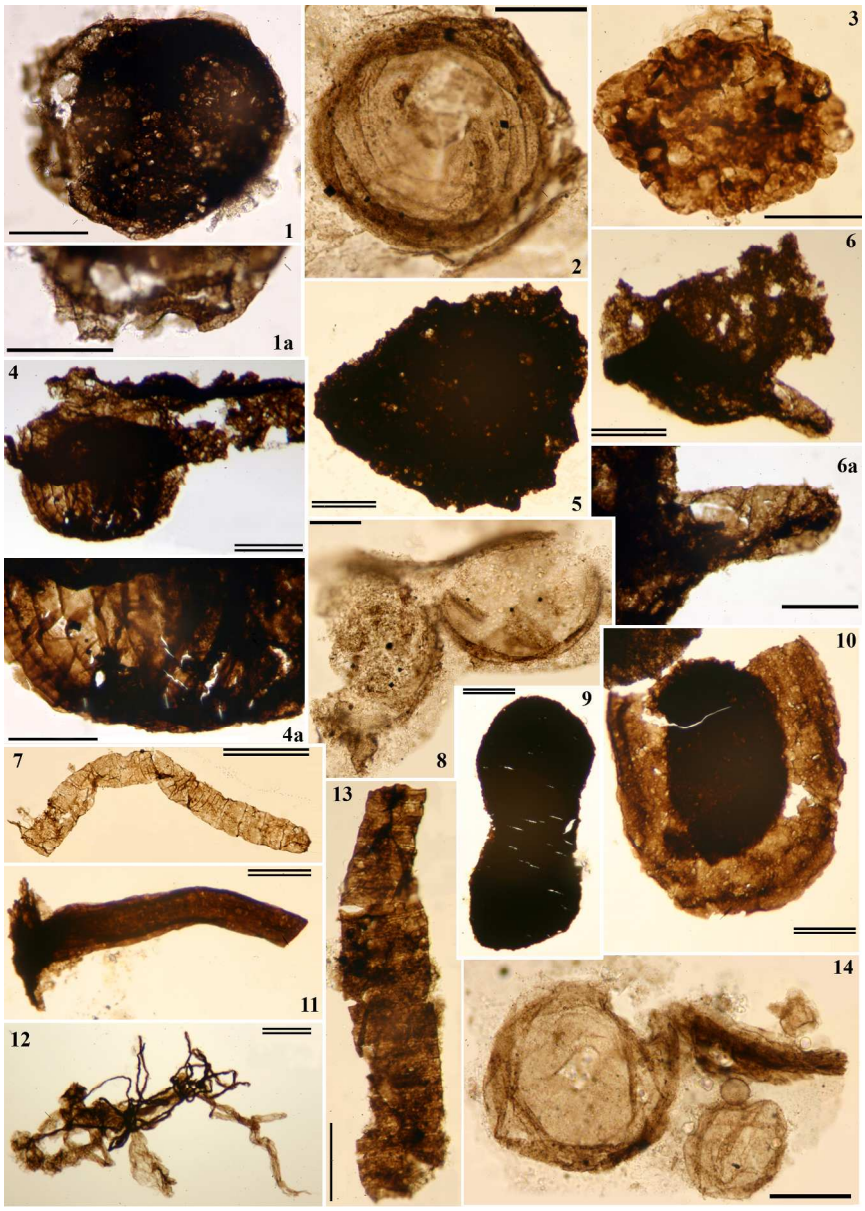

199x280mm (300 x 300 DPI)

	Samples		
Biomarker Ratios	**BA203-3452**	**BA203-4201.5**	**BA203-4390**
C_{31} S/(S+R) hopane	0.54	0.55	0.55
Ts/(Ts + Tm)	0.49	0.56	0.58
C_{26}/C_{25} tricyclic	0.00	0.82	0.30
$C_{31}R/C_{30}$ hopane	0.37	0.33	0.44
C_{24}/C_{23} tricyclic	0.43	0.38	0.31
C_{22}/C_{21} tricyclic	0.00	0.43	0.44
C_{31} hopane/(total hopane)	0.17	0.20	0.23
C_{32} hopane/(total hopane)	0.11	0.13	0.16
C_{33} hopane/(total hopane)	0.09	0.05	0.08
C_{34} hopane/(total hopane)	0.05	0.04	0.04
C_{35} hopane/(total hopane)	0.05	0.05	0.04
28,30-DNH/C_{30} hopane	0.09	0.09	0.17